High-power spectral beam combining of linearly polarized Tm:fiber lasers

Lawrence Shah,[1,*] R. Andrew Sims,[1,2] Pankaj Kadwani,[1,3] Christina C.C. Willis,[1,4] Joshua B. Bradford,[1] Alex Sincore,[1] and Martin Richardson[1]

[1]Townes Laser Institute, CREOL, The College of Optics and Photonics, University of Central Florida, Orlando, Florida 32816, USA

[2]Currently at Lockheed Martin Coherent Technologies, Louisville, Colorado 80027, USA

[3]Currently at IPG Photonics Corporation, Oxford, Massachusetts 01540, USA

[4]Currently at Fibertek Inc., Herndon, Virginia 20171, USA

*Corresponding author: lshah@creol.ucf.edu

Received 16 September 2014; revised 12 December 2014; accepted 15 December 2014; posted 17 December 2014 (Doc. ID 223099); published 26 January 2015

To date, high-power scaling of Tm:fiber lasers has been accomplished by maximizing the power from a single fiber aperture. In this work, we investigate power scaling by spectral beam combination of three linearly polarized Tm:fiber MOPA lasers using dielectric mirrors with a steep transition from highly reflective to highly transmissive that enable a minimum wavelength separation of 6 nm between individual laser channels within the wavelength range from 2030 to 2050 nm. Maximum output power is 253 W with $M^2 < 2$, ultimately limited by thermal lensing in the beam combining elements.

OCIS codes: (140.3298) Laser beam combining; (140.3510) Lasers, fiber; (060.2390) Fiber optics, infrared.

http://dx.doi.org/10.1364/AO.54.000757

1. Introduction

Average powers as high as 1 kW have been demonstrated in Thulium fiber lasers [1] along with high-power narrow-linewidth output [2–6], wavelength tunability [3,7,8], and all-fiber architecture [1,4–6]. Additionally, there have been recent advances in high-power Holmium doped fiber lasers [9,10] as well as several notable improvements in pulsed Tm:fiber laser performance in nanosecond [11–13], picosecond [14,15], and femtosecond [16–19] regimes for use in a wide range of applications such as pumps for mid-IR generation, LIDAR, materials processing, and telecommunications.

For many such applications, high average power and/or high peak power are highly desirable. To supplement ongoing work on scaling Tm:fiber performance from a single aperture, this work aimed to improve upon previous spectral beam combining (SBC) work at 2 μm wavelength [20,21] to maximize average power and spectral density within the window from 2030 to 2050 nm corresponding to a local maximum in atmospheric transmission.

In [21], we achieved a maximum combined power of 48 W using a ruled gold-coated reflective diffraction grating as the combining element. Power scaling in these experiments was limited by three factors: low combining efficiency due to the use of a polarization sensitive combining element with nonpolarized sources; the dependence of the combined beam quality on the spectral purity/stability of the laser sources; and beam quality degradation resulting

1559-128X/15/040757-06$15.00/0

from induced thermal distortion of the grating. In this work, the first issue was solved by employing linearly polarized Tm:fiber master oscillator power amplifier (MOPA) lasers, producing 100 W with $M^2 < 1.5$ [22]. Using nondiffractive combining elements, inspired by [23–25], solved the second issue. However, thermal lensing in the SBC elements remains the current fundamental on power scalability. Although this work does not match the output power of previous efforts [1,2,10], it highlights significant recent improvement in the performance of high-power 2 μm fiber lasers and associated components. Significant reductions in thermal load are required to approach the average power of Yb:fiber systems. This is true in terms of improving efficiency in Tm- and Ho-doped fibers as well as passive component absorption at 2 μm and the associated performance limits imposed by the thermal-optic response.

2. Experimental Setup

The Tm:fiber MOPA systems in this study utilize single-mode fiber in the oscillators and large mode area (LMA) fibers in the amplifiers, as shown in Fig. 1 and originally reported in [22]. In each oscillator, the wavelength and polarization were locked using an individual guided mode resonance filter [26,27], such that the wavelengths of MOPAs 1, 2, and 3 are centered at 2046.6, 2040.7, and 2034.6 nm, respectively. As part of this work, we also utilized oscillators in which we replaced the free-space portion of the cavity with an in-line polarizer and a narrow wavelength fiber Bragg grating to make the system "all-fiber." However, the free-space configuration provided greater flexibility to change the wavelength of the oscillators and was used for the results reported here.

The SBC setup is shown in Fig. 2, illustrating the beam paths for MOPAs 1, 2, and 3, respectively. As shown, the beams from MOPA 2 and 3 are added sequentially to the MOPA 1 beam using wavelength selective mirrors. This approach is well established for wavelength division multiplexing particularly at 1.5 μm; however, to our knowledge this is the first

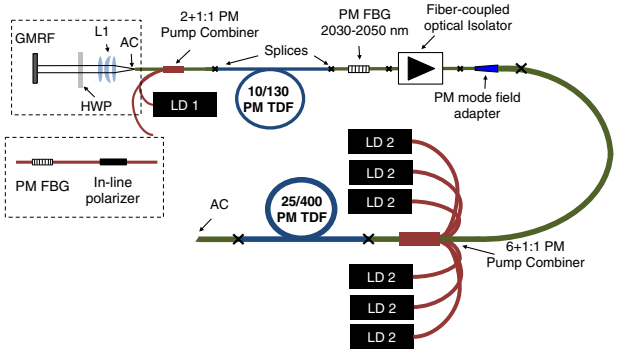

Fig. 1. Tm:fiber MOPA schematic where HWP is a half-wave plate, L1 is a 26 mm focal length Infrasil triplet, AC is a angle-cleaved fiber facet, LD1 is a 35 W 793 nm diode, LD2 are each 70 W 793 nm diodes; the free-space portion of the standard cavity is outlined in upper dashed box and could be replaced by the lower dashed box to make an "all-fiber" MOPA [22].

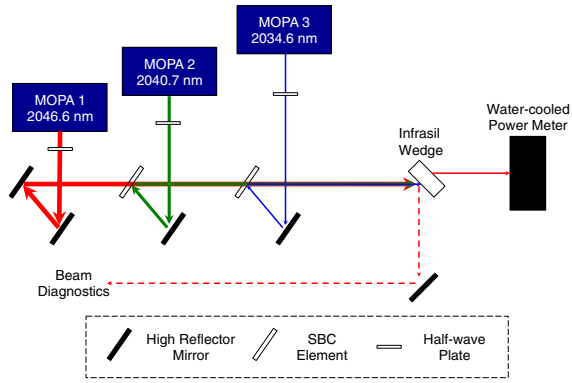

Fig. 2. Schematic of SBC beam paths.

application of this technology for high-power SBC at 2 μm wavelength.

3. Results

The output spectra of the three MOPAs are shown in Fig. 3, with ~6 nm wavelength separation and >30 dB optical signal-to-noise ratio. The <30 GHz bandwidth of each channel is sufficient for tighter wavelength spacing despite being much wider than single-frequency; however, the minimum wavelength separation is set by the SBC elements.

The SBC elements described here, designed/fabricated by CVI/MellesGriot, are a modified version of commercial filters for wavelength division multiplexing at 1.5 μm and utilize coatings consisting of a large number of dielectric layers to achieve a sharp transition from highly reflective to highly transmissive. Magnetron sputtering was used to deposit a high-density coating in order to avoid infiltration of humidity over time. The proprietary fabrication process has been developed for WMS-15 glass-ceramic substrates, and, unfortunately, re-engineering the dielectric coating "recipe" for a substrate more optimal for use at 2 μm was not possible as part of this work.

Figure 4 shows the steepness of the transition, measured using a homemade Tm:fiber amplified spontaneous emission (ASE) source and an optical spectrum analyzer (Yokogawa AQ6375). At 22°

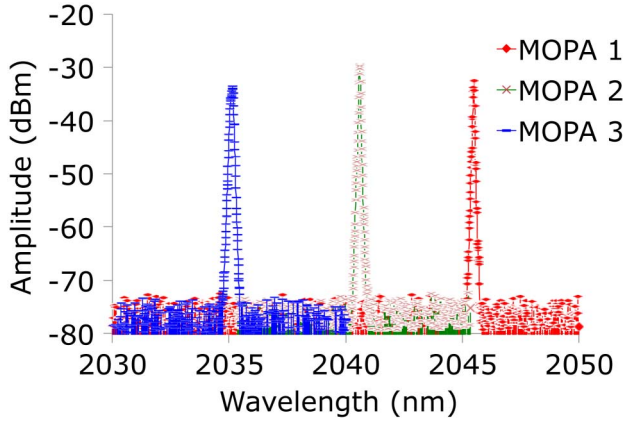

Fig. 3. Spectrum of combined beam MOPA 1 at 2046.6 nm, MOPA 2 at 2040.7 nm, and MOPA 3 at 2034.6 nm.

AOI, the transition width is ~5 nm and is polarization dependent (Fig. 4); hence, the need for linearly polarized wavelength channels. By slightly changing the AOI, the transition wavelength can be shifted to cover the wavelength range from 2030–2050 nm. The measurement noise at >2030 nm is the result of the ASE source being centered at ~1970 nm and having relatively low spectral brightness at longer wavelengths.

The power amplifier output power versus the 790 nm diode pump power for each MOPA is shown in Fig. 5. The slope efficiency of each system is >40%, demonstrating cross relaxation [28], but notably lower than the >60% slope achieved in [8]. As described in [22], the length of active Tm:fiber was optimized for the wavelength of operation and cooled as required for high efficiency [29]. As such, two factors are primarily responsible for the reduced efficiency. The copropagating pump geometry was chosen to reduce the risk of damage to the pump combiner, although this comes at the expense of ~5–10% efficiency relative to counterpropagating pump, as demonstrated in [4]. The 2030–2050 nm band is near the long wavelength limit of Tm:fiber tunability [7,8] and, similarly, leads to a reduction in system efficiency relative to systems operating ~1950–2000 nm.

Finally, the performance of the MOPA systems is very sensitive to the splices between the passive and active portions of the polarization maintaining (PM) LMA fibers (Nufern PLMA-GDF-25/400-10FA and PLMA-TDF-25P/400-HE). These fibers are inherently multimode; therefore, very small splice variations in the amount of higher order mode (HOM) content lead to variations in beam quality and efficiency of the individual units. Furthermore, these PM fibers have larger HOM content [22] than reported for non-PM fiber by [2,8]. Likewise, the performance of the tapered fiber bundle pump combiner is significantly affected by the use of PM fiber. Most obviously, the maximum power handling of the combiners used in [1] is significantly higher than reported in [4,6, and 22].

The output power of each MOPA was limited to 100 W to minimize the chance of damage to the PM tapered fiber bundle pump combiners, although higher powers have been demonstrated with similar amplifier configurations [4,6]. Each amplifier output was collimated to 3 mm ($FW1/e^2M$) beam diameter using a 26 mm focal length Infrasil triplet lens AR coated for 2.0–2.1 μm. Half-wave plates on each laser were used to align polarization, prior to beam combining. The alignment of each MOPA system required slight adjustment relative to output power due to heating of the collimating lens/mount from residual pump light that could not be filtered. Once the systems reached thermal equilibrium (~5–10 min after changing power), the centroid of the beam was stable with an overall pointing fluctuation measured to be <100 μrad for the individual MOPAs independent of output power.

The total output power and the combined beam power are plotted in Fig. 6 versus the total pump power. The combining efficiency does not degrade with increasing power to the maximum combined power of 253 W, from 284 W total output. The combining efficiency was primarily limited by the maximum transmission of the SBC elements. Figure 4 shows the maximum transmission is limited to <98%, and the maximum reflection is <99%, such that the maximum possible combining efficiency for this setup is ~96%. The shoulders of the transition extend to ~10 nm further increasing SBC losses and/or limiting spectral density. The sharpness of the transition is proportional to the number of layers in the dielectric coating stack; however, further increasing the number of layers is technically infeasible due to increased stress/strain in the coating as well as between the coating and the substrate. As such, the 6 nm wavelength spacing was chosen, as it provided the best compromise between combining efficiency and spectral density.

Near-field beam images at full power are shown in Fig. 7, illustrating the beam quality for each individual and the combined beam. The output beam quality of MOPA 3, with an M^2 of ~1.4, is notably worse than

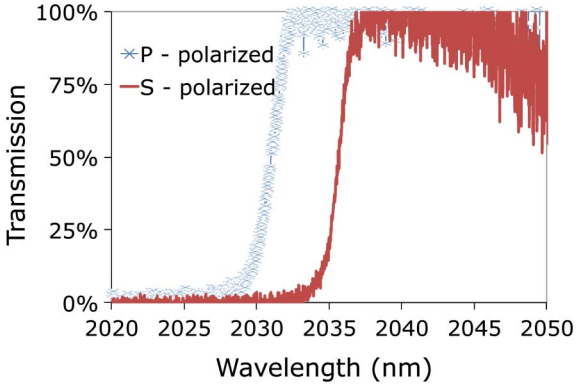

Fig. 4. Measured reflectivity transition edge of SBC elements.

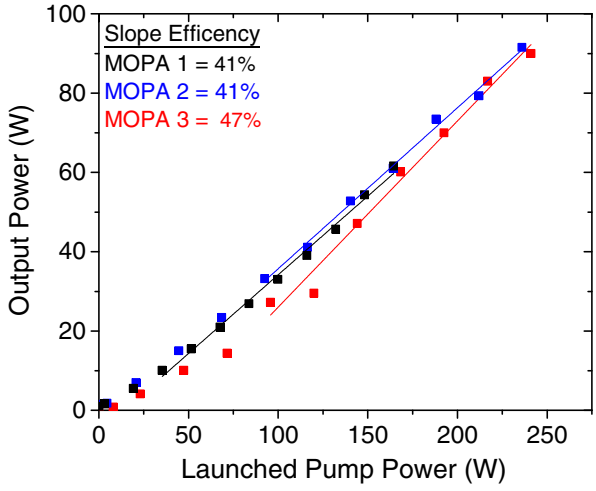

Fig. 5. Output power relative to pump power and slope efficiencies for MOPAs 1, 2, and 3.

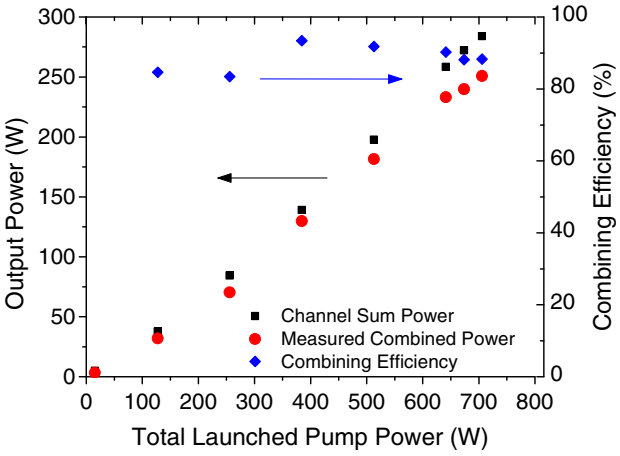

Fig. 6. Total output power, combined output power, and combining efficiency relative to launched pump power.

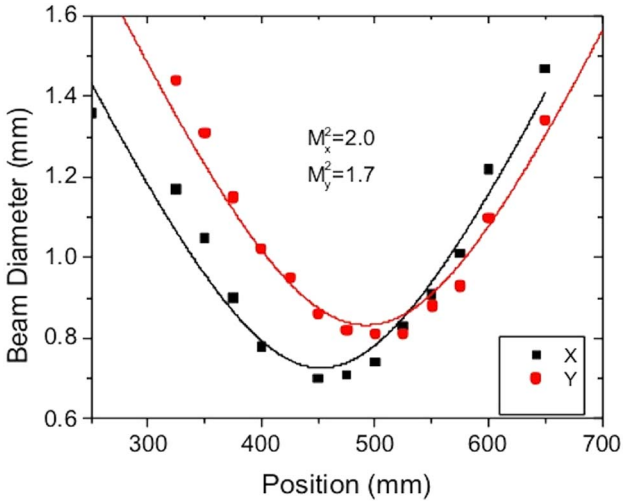

Fig. 8. Measured M^2 data for the combined beam at full power.

MOPAs 1 and 2, with M^2 of 1.2–1.25. This further illustrates the tendency of the PM LMA fiber to suffer from HOM content. The impact of HOM content on beam quality is particularly evident if the amplifier fiber is mechanically perturbed or while the amplifier is reaching thermal equilibrium. Despite the multimode output, the M^2 for each MOPA remains $\leq$1.5, does not degrade with increased power, and is stable for fixed pump power.

The M^2 data for the combined SBC beam at full power is shown in Fig. 8. The combined beam quality is worse, with higher asymmetry and astigmatism, than the individual beams, while the overall beam quality is still high ($M^2 < 2$). This could not be further improved by adjusting the alignment or beam divergence of the individual lasers; therefore, it was not possible to match $M^2 < 1.5$ of the MOPAs prior to beam combination. Pointing stability does not appear to influence this reduction in beam quality, as the motion of the combined beam was found to be equivalent to that for the individual beams. However, as part of M^2 measurements, it was seen that the location of the beam waist shifted slightly for combined power >225 W. No such shift was observed for the MOPAs individually. As such, the primary limitation to power scaling in these experiments is beam quality degradation during beam combination.

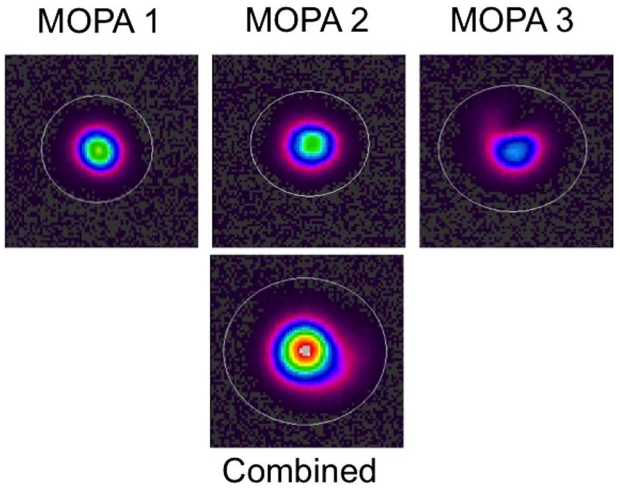

Fig. 7. Near-field beam profiles for MOPAs 1, 2, and 3 individually and combined at full power.

4. Discussion

Given that the degradation in performance affected beam quality but not combining efficiency or pointing stability, thermal lensing was suspected. To provide a relative measure of thermal effects in our SBC setup, we utilized a Shack–Hartman wavefront sensor and a probe beam to compare the thermal lens induced in our SBC elements to uncoated BK7, UV fused silica, and Infrasil windows. Silica glass with low OH content, such as Infrasil, is preferable for transmissive optics as the absorption at 2 μm is minimal; however, many off-the-shelf optics utilize nonoptimal substrates similar to BK7 and UV fused silica.

Each sample was placed in the combined beam with a beam diameter of 3 mm and irradiated with up to 240 W. The focal length of the induced thermal lens is plotted as a function of incident power in Fig. 9. No thermal lensing was measureable for Infrasil, while BK7 and UV-grade fused silica exhibit

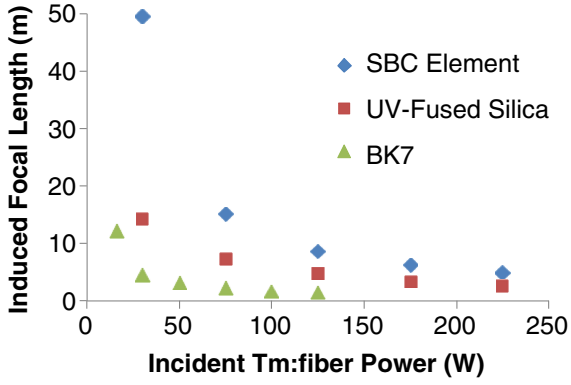

Fig. 9. Thermal lens induced focal length.

relatively strong thermal lensing, as expected. Based on these measurements, the focal length of the induced thermal lens in the SBC elements is 7–10 m as configured in Fig. 1, which matches well with the observed degradation in beam quality at the maximum combined power.

In this case, the performance of the SBC elements is fundamentally limited by the WMS-15 substrate. The absorption is eight times larger at 2 μm, and the thermal expansion coefficient is over 20 times larger [30] than for an optimal silica glass substrate such as Suprasil 3001 [31]. The overall thermal response is moderated by the negative dn/dT of WMS-15 [30]; however, it is still ~10 times larger than silica glass with low OH content. As such, the level of thermal distortion observed in this work would occur at kilowatt average powers in a more optimal substrate.

Unfortunately, the Pockels coefficient was not available from the manufacturer to calculate the substrate photoelastic stress, and the stress/strain associated with the coating cannot be directly determined at this time. While thermal expansion is the dominant effect for WMS-15, stress and strain are likely more important for substrates with lower absorption, as the choice of substrate will influence the stress/strain inherent in the structure of dielectric coating and will significantly decrease the thermo-optic impact of the substrate relative to the coating and the substrate/coating interface. As such, it is difficult to accurately determine the limits on power scaling this approach to SBC at 2 μm wavelength; however, scalability to >10 kW average power level appears possible.

5. Conclusion

This article reviews high-power SBC of Tm:fiber lasers at 2 μm wavelength, achieving a maximum combined power of 253 W with 89% efficiency and $M^2 < 2$. Further power scaling using the approach in this work is limited in two fundamental ways. First, the power of a single MOPA channel is currently practically limited to ~200 W [5], as highly polarized output is desirable for this application. Second, and more fundamentally, thermal induced beam distortions in the SBC elements limit power scalability due to high absorption at 2 μm and large thermo-optic response relative to more optimal silica glass substrates with low OH content.

This work demonstrates that improvements in substrates and edge filter dielectric coatings will enable this SBC technique to be scaled to multi-kW average powers; however, this work also highlights that high-power component development at 2 μm is still significantly less mature than for 1 μm. Similar and more extreme challenges are associated with the development of optical systems for high-power applications in the mid-IR.

This work was supported by the United States High Energy Laser Joint Technology Office (HEL-JTO) through contracts with the United States Air Force Office of Scientific Research (AFOSR) contract numbers FA945110D0234 and FA95501010543, and the United States Army Research Office (ARO) contract number W911NF12R003, as well as the state of Florida.

References

1. T. Ehrenreich, R. Leveille, I. Majid, K. Tankala, G. Rines, and P. Moulton, "1-kW, all-glass Tm:fiber laser," Proc. SPIE **7580**, 7580112 (2010).
2. G. D. Goodno, L. D. Book, and J. E. Rothenberg, "Low-phase-noise, single-frequency, single-mode 608 W thulium fiber amplifier," Opt. Lett. **34**, 1204–1206 (2009).
3. L. Pearson, J. W. Kim, Z. Zhang, M. Ibsen, J. K. Sahu, and W. A. Clarkson, "High-power linearly-polarized single-frequency thulium-doped fiber maser-oscillator power-amplifier," Opt. Express **18**, 1607–1612 (2010).
4. Y. Tang, C. Huang, S. Wang, H. Li, and J. Xu, "High-power narrow-bandwidth thulium fiber laser with an all-fiber cavity," Opt. Express **20**, 17539–17544 (2012).
5. X. Wang, P. Zhou, X. Wang, H. Xia, and L. Si, "102 W monolithic single frequency Tm-doped fiber MOPA," Opt. Express **21**, 32386–32392 (2013).
6. J. Liu, H. Shi, K. Liu, Y. Hou, and P. Wang, "210 W single-frequency, single-polarization, thulium-doped all-fiber MOPA," Opt. Express **22**, 13572–13578 (2014).
7. W. A. Clarkson, N. P. Barnes, P. W. Turner, J. Nilsson, and D. C. Hanna, "High-power cladding-pumped Tm-doped silica fiber laser with wavelength tuning from 1860 to 2090 nm," Opt. Lett. **27**, 1989–1991 (2002).
8. T. S. McComb, R. A. Sims, C. C. C. Willis, P. Kadwani, V. Sudesh, L. Shah, and M. C. Richardson, "High-power, widely tunable thulium fiber lasers," Appl. Opt. **49**, 6236–6242 (2010).
9. A. Hemming, S. Bennetts, N. Simakov, A. Davidson, J. Haub, and A. Carter, "High power operation of cladding pumped holmium-doped silica fibre lasers," Opt. Express **21**, 4560–4566 (2013).
10. A. Hemming, N. Simakov, A. Davidson, S. Bennetts, M. Hughes, N. Carmody, P. Davies, L. Corena, D. Stepanov, J. Haub, R. Swain, and A. Carter, "A monolithic cladding pumped holmium-doped fibre laser," in *Conference on Lasers and Electro-Optics (CLEO)*, OSA Technical Digest (online) (Optical Society of America, 2013), paper CW1M.1.
11. Q. Fang, W. Shi, K. Kieu, E. Petersen, A. Chavez-Pirson, and N. Peyghambarian, "High power and high energy monolithic single frequency 2 μm nanosecond pulsed fiber laser by using large core Tm-doped germanate fibers: experiment and modeling," Opt. Express **20**, 16410–16420 (2012).
12. C. Gaida, M. Gebhardt, P. Kadwani, L. Leick, J. Broeng, L. Shah, and M. Richardson, "Amplification of nanosecond pulses to megawatt peak power levels in Tm^{3+}-doped photonic crystal fiber rod," Opt. Lett. **38**, 691–693 (2013).
13. F. Stutzki, F. Jansen, C. Jauregui, J. Limpert, and A. Tünnermann, "2.4 mJ, 33 W Q-switched Tm-doped fiber laser with near diffraction-limited beam quality," Opt. Lett. **38**, 97–99 (2013).
14. J. Liu, Q. Wang, and P. Wang, "High average power picosecond pulse generation from a thulium-doped all-fiber MOPA system," Opt. Express **20**, 22442–22447 (2012).
15. A. M. Heidt, Z. Li, J. Sahu, P. C. Shardlow, M. Becker, M. Rothhardt, M. Idbsen, R. Phelan, B. Kelly, S. U. Alam, and D. J. Richardson, "100 kW peak power picosecond thulium-doped fiber amplifier system seeded by a gain-switched diode laser at 2 μm," Opt. Lett. **38**, 1615–1617 (2013).
16. J. Bethge, J. Jiang, C. Mohr, M. Fermann, and I. Hartl, "Optically referenced Tm-fiber-laser frequency comb," in *Lasers, Sources, and Related Photonic Devices*, OSA Technical Digest (CD) (Optical Society of America, 2012), paper AT5A.3.
17. R. A. Sims, P. Kadwani, A. Sincore, L. Shah, and M. Richardson, "1 μJ, sub-500 fs chirped pulse amplification in a Tm-doped fiber system," Opt. Lett. **38**, 121–123 (2013).
18. P. Wan, L.-M. Yang, and J. Liu, "High pulse energy 2 μm femtosecond fiber laser," Opt. Express **21**, 1798–1803 (2013).

19. F. Stutzki, C. Gaida, M. Gebhardt, F. Jansen, A. Wienke, U. Zeitner, F. Fuchs, C. Jauregui, D. Wandt, D. Kracht, J. Limpert, and A. Tünnermann, "152 W average power Tm-doped fiber CPA system," Opt. Lett. **39**, 4671–4674 (2014).
20. W. A. Clarkson, V. Matera, A. M. Abdolvand, T. M. J. Kendall, D. C. Hanna, J. Nilsson, and P. W. Turner, "Spectral beam combining of cladding-pumped Tm-doped fibre lasers," in *QEP-15*, Glasgow, UK, 2001.
21. R. A. Sims, C. C. C. Willis, P. Kadwani, T. S. McComb, L. Shah, V. Sudesh, Z. Roth, M. K. Poutous, E. G. Johnson, and M. Richardson, "Spectral beam combining of 2 μm Tm fiber laser systems," Opt. Commun. **284**, 1988–1991 (2011).
22. L. Shah, R. A. Sims, P. Kadwani, C. C. C. Willis, J. B. Bradford, A. Pung, M. K. Poutous, E. G. Johnson, and M. Richardson, "Integrated Tm:fiber MOPA with polarized output and narrow linewidth with 100 W average power," Opt. Express **20**, 20558–20563 (2012).
23. K. Regelskis, K. Hou, G. Raciukaitis, and A. Galvanauskas, "Spatial-dispersion-free spectral beam combining of high power pulsed Yb-doped fiber lasers," in *Conference on Lasers and Electro-Optics/Quantum Electronics and Laser Science Conference and Photonic Applications Systems Technologies*, OSA Technical Digest (CD) (Optical Society of America, 2008), paper CMA4.
24. A. Sevian, O. Andrusyak, I. Ciapurin, V. Smirnov, G. Venus, and L. Glebov, "Efficient power scaling of laser radiation by spectral beam combining," Opt. Lett. **33**, 384–386 (2008).
25. O. Schmidt, C. Wirth, D. Nodop, J. Limpert, T. Schreiber, T. Perschel, R. Eberhardt, and A. Tünnermann, "Spectral beam combination of fiber amplified ns-pulses by means of interference filters," Opt. Express **17**, 22975–22982 (2009).
26. M. A. Duguay, Y. Kokubun, T. L. Koch, and L. Pfeiffer, "Antiresonant reflecting optical waveguides in SiO_2-Si multilayered structures," Appl. Phys. Lett. **49**, 13–15 (1986).
27. R. A. Sims, Z. A. Roth, C. C. Willis, P. Kadwani, T. S. McComb, L. Shah, C. Sudesh, M. Poutous, E. G. Johnson, and M. Richardson, "Spectral narrowing and stabilization of thulium fiber lasers using guided-mode resonance filters," Opt. Lett. **36**, 737–739 (2011).
28. S. D. Jackson, "Cross relaxation and energy transfer upconversion processes relevant to the functioning of 2 μm Tm^{3+}-doped silica fibre lasers," Opt. Commun. **230**, 197–203 (2004).
29. G. P. Frith and D. G. Lancaster, "Power scalable and efficiency 790 nm pumped Tm^{3+}-doped fibre lasers," Proc. SPIE **6102**, 610208 (2006).
30. C. Ghio, Ohara Corporation (personal communication, 2014).
31. Heraeus Suprasil 3001 and 3002 retrieved from http://optics.heraeus-quarzglas.com/media/webmedia_local/datenbltter/Suprasil_3001_3002_puritysyntheticfusedsilica.pdf.